AIAA 2002-0262
Effects of Constant Turbulent Eddy Viscosity Assumption on Gradient-Based Design Optimization

Chang Sung Kim
Institute of Advanced Design and Machinery
Seoul National University, Seoul 151-742, Korea

Chongam Kim and Oh-Hyun Rho
Department of Aerospace Engineering
Seoul National University, Seoul 151-742, Korea

40th AIAA Aerospace Sciences Meeting & Exhibit
January 14-17, 2002/Reno, NV

AIAA 2002-0262

Effects of Constant Turbulent Eddy Viscosity Assumption on Gradient-Based Design Optimization

Chang Sung Kim,* Chongam Kim,† and Oh Hyun Rho‡
Seoul National University, Seoul 151-742, Republic of Korea

Abstract

A feasibility study is carried out by investigating the effects of a usual assumption of constant turbulent eddy viscosity on the aerodynamic design using an adjoint variable method, one of most efficient gradient-based optimization techniques. Accurate steady and unsteady flow analyses are followed by the aerodynamic sensitivity analysis for the Navier-Stokes equations coupled with two-equation turbulence models. The capability of the present sensitivity analysis code to treat complex geometry using the chimera overlaid grid is also demonstrated by analyzing the flow over multielement airfoil. Like the mean flow equations, the turbulence model equations are also hand-differentiated to accurately calculate the sensitivity derivatives of flow quantities in turbulent viscous flows. With two-equation turbulence models, it is observed that the constant turbulent eddy viscosity assumption in the adjoint variable method could lead to inaccurate results in several test cases of transonic airfoil with strong shock and multielement airfoil at high angle of attack. Especially for the flow over high-lift airfoil close to stall, both flow analysis and sensitivity analysis are performed in an unsteady, time-accurate manner using the dual time stepping method. In addition, the effects of constant eddy viscosity assumption on single and multielement airfoil design optimization are carefully investigated in various design examples.

Introduction

As computational power advances, design optimization tools using computational fluid dynamics (CFD) have played a more important role in aerodynamic design. Among advanced optimization techniques, gradient-based optimization method has been widely used and even applied to multidisciplinary design optimization (MDO). In general, a gradient-based design optimization requires two steps. The first is to obtain the search direction that defines how the design variables will be changed for design improvement. The second is, so called one-dimensional search, to determine how far the design variables will move in this direction. This basic process is repeated until it approaches to the optimum.

In one-dimensional search, an accurate and efficient flow solver is indispensable for the computation of pressure distribution and aerodynamic load coefficients such as lift, drag and pitching moment which are used in an objective function to be either minimized or maximized. Especially for the high-lift design optimization, it was previously noted that the unsteady, time-accurate computation is definitely required for the accurate computation of the flow over a high-lift device at a higher angle of attack close to stall angle where massive flow separation might occur.[1]

In determining the search direction, the gradients of design variables were traditionally calculated by the finite-difference method. It is, however, too expensive to compute the flow field iteratively with the incremented values of a design variable for complex two-dimensional or three-dimensional problems. In addition, this method is so sensitive to the step size of a design variable that it sometimes provides inaccurate signs or sensitivity derivatives.[2-4] Therefore, more robust techniques have been proposed using direct differentiation methods and adjoint variable methods.[4-12] Compared with the direct differentiation methods, the adjoint variable methods are more advantageous for their capability to compute the gradients of the objective function and constraints when the number of design variables is much larger than that of the objective function and constraints. The adjoint variable methods adopt the formulation of the gradient in either a discrete or a continuous approach. In the discrete approach, which is used in the present work, the discretized governing equations are differentiated with respect to design variables whereas the adjoint equations are first differentiated and

* Postdoctorial Researcher, Institute of Advanced Machinery and Design, AIAA Member.
† Assistant Professor, Dep't of Aerospace Engineering, AIAA Member.
‡ Professor, Dep't of Aerospace Engineering, AIAA Senior Member.

then discretized in the continuous approach. [9, 10]

It is necessary to incorporate the effect of turbulence in differentiating the governing equations to treat high Reynolds number flows more accurately. It is, however, very difficult to fully hand-differentiate the governing equations including the viscous terms and turbulence terms. Thus, some software tools such as automatic differentiation[7, 8, 11] are used for the Navier-Stokes equations with a turbulence model. However, this approach is generally less efficient, in terms of computing time and computer memory, than hand-differentiation codes.[7, 12] In the present work, the Navier-Stokes equations coupled with two-equation turbulence models are fully differentiated by human hand. Among most popular two-equation turbulence models[13-16], the $k-\omega$ SST model[13, 14] is mainly used and then compared with the original $k-\omega$ model[15, 16] and the standard $k-\varepsilon$ model[14]. Like the mean flow equations, the turbulence model equations are also hand-differentiated to accurately compute the sensitivity derivatives of flow quantities with respect to design variables in turbulent flows.

A usual assumption of constant turbulent eddy viscosity (CTEV, hereafter) in the adjoint variable methods has been previously used in aerodynamic design optimizations [9, 10]. Recently, the accuracy of this assumption in sensitivity analysis for turbulent flows was reported using two-equation turbulence models on chimera overlaid grids and a one-equation turbulence model on unstructured grids in Refs. 2 and 4, respectively. In the present study, the feasibility of constant eddy viscosity assumption is carefully studied by comparing the sensitivity gradients using the CSAAV code[2], and the effects of this assumption on single and multielement airfoil design optimization are further investigated in various design examples: subsonic and transonic designs for drag minimization and lift maximization, and high-lift designs for lift to drag ratio maximization and even $Cl_{\max}$ maximization.

Numerical Background

Flow Analysis

The Compressible Flow Analysis Navier-Stokes (CFANS2D/3D) solver, which has been well verified in many applications[1, 2, 17], is used for the computation of turbulent viscous flows over single and multielement airfoils. The governing equations are the two-dimensional, unsteady, compressible Navier-Stokes equations coupled with two-equation turbulence models: the $k-\omega$ SST model[13, 14], the $k-\omega$ model[15, 16], and the standard $k-\varepsilon$ model[14]. The governing equations are transformed in generalized coordinates and are solved with a finite-volume method. Using a backward Euler implicit method, the governing equations adopting the dual time stepping method are discretized in time and linearized in delta form as:

$$\left[\frac{I}{J\Delta\tau}+\left(\frac{\partial R_s}{\partial Q}+\frac{\partial S}{\partial Q}\right)^{n+1,m}\right]\Delta Q^{n+1,m+1}=-(R_s+S)^{n+1,m}=-R^{n+1,m}, \quad (1)$$

$$S^{n+1}=\frac{1.5Q^{n+1}-2Q^{n}+0.5Q^{n-1}}{J\Delta t}$$

where J is the Jacobian of transformation, τ and superscript m represent pseudo time while t and n for physical time. R_s and S are the residual of the steady-state flow equations and unsteady source-like term respectively, and Q is the 6-element vector of conservative variables $(\rho, \rho u, \rho v, \rho E, \rho k, \rho\omega)^T$.

For the calculation of the residual, convective terms are upwind-differenced based on Roe's Flux Difference Splitting (FDS) scheme[18] and viscous terms are central-differenced. A MUSCL (Monotone Upstream Centered Scheme for Conservation Laws) approach using a third order interpolation is used to obtain a higher order of spatial accuracy. [19] The third order of spatial accuracy is kept in all calculations. For a temporal integration, Yoon and Kwak's LU-SGS scheme[20] is adopted to efficiently solve Eq. (1). Wall boundary conditions are applied explicitly with the non-slip condition. For inflow and outflow boundaries, characteristic conditions based on one-dimensional Riemann invariants are imposed. For the Chimera grid scheme, a bilinear interpolation that was known to be robust and easy to implement is adopted for the hole-cutting boundary.[1, 17]

Aerodynamic Sensitivity Analysis

The discrete residual of the unsteady flow equations can be written as:

$$\{R\}=\{R_s\}+\{S\}=R\{Q,X,D\}=\{0\} \quad (2)$$

where X is the computational grid position and D is the vector of design variables. Similarly, the vector of the aerodynamic objective function F to be either minimized or maximized is also dependent on Q, X and D as:

$$\{F\}=\{F(Q,X,D)\} \quad (3)$$

Sensitivity derivatives of the aerodynamic functions are calculated by directly differentiating Eqs. (2) and (3) with respect to D as:

$$\left\{\frac{dR}{dD}\right\}=\left[\frac{\partial R}{\partial Q}\right]\left\{\frac{dQ}{dD}\right\}+\left[\frac{\partial R}{\partial X}\right]\left\{\frac{dX}{dD}\right\}+\left\{\frac{\partial R}{\partial D}\right\}=\{0\} \quad (4)$$

$$\left\{\frac{dF}{dD}\right\}=\left[\frac{\partial F}{\partial Q}\right]^T\left\{\frac{dQ}{dD}\right\}+\left[\frac{\partial F}{\partial X}\right]^T\left\{\frac{dX}{dD}\right\}+\left\{\frac{\partial F}{\partial D}\right\} \quad (5)$$

In the adjoint variable (AV) method, the sensitivity derivatives of the aerodynamic functions are obtained by combining Eqs. (4) and (5) as:

$$\left\{\frac{dF}{dD}\right\}=\left\{\frac{\partial F}{\partial Q}\right\}^T\left\{\frac{dQ}{dD}\right\}+\left\{\frac{\partial F}{\partial X}\right\}^T\left\{\frac{dX}{dD}\right\}+\left\{\frac{\partial F}{\partial D}\right\} + \Lambda^T\left(\left[\frac{\partial R}{\partial Q}\right]\left\{\frac{dQ}{dD}\right\}+\left[\frac{\partial R}{\partial X}\right]\left\{\frac{dX}{dD}\right\}+\left\{\frac{\partial R}{\partial D}\right\}\right) \tag{6}$$

where Λ represents the 6-element adjoint vector of Lagrangian multipliers $(\lambda_1,\lambda_2,\lambda_3,\lambda_4,\lambda_5,\lambda_6)^T$ corresponding to the conservative variables $(\rho,\rho u,\rho v,\rho E,\rho k,\rho\omega)^T$. The geometric sensitivity vector $\{dX/dD\}$ can be calculated by differentiating the grid generation code. In the present work, the finite difference approximation is applied for simplicity. Rearranging Eq. (6) yields the following equation.

$$\left\{\frac{dF}{dD}\right\}=\left\{\frac{\partial F}{\partial X}\right\}^T\left\{\frac{dX}{dD}\right\}+\left\{\frac{\partial F}{\partial D}\right\}+\Lambda^T\left(\left[\frac{\partial R}{\partial X}\right]\left\{\frac{dX}{dD}\right\}+\left\{\frac{\partial R}{\partial D}\right\}\right) + \left(\left\{\frac{\partial F}{\partial Q}\right\}^T+\Lambda^T\left[\frac{\partial R}{\partial Q}\right]\right)\left\{\frac{dQ}{dD}\right\} \tag{7}$$

Without evaluating the vector $\{dQ/dD\}$, the sensitivity derivatives of the aerodynamic functions can be calculated as:

$$\left\{\frac{dF}{dD}\right\}=\left\{\frac{\partial F}{\partial X}\right\}^T\left\{\frac{dX}{dD}\right\}+\left\{\frac{\partial F}{\partial D}\right\}+\Lambda^T\left(\left[\frac{\partial R}{\partial X}\right]\left\{\frac{dX}{dD}\right\}+\left\{\frac{\partial R}{\partial D}\right\}\right) \tag{8}$$

if and only if the arbitrary vector Λ satisfies the following adjoint equation.

$$\left[\frac{\partial R}{\partial Q}\right]^T\Lambda+\left\{\frac{\partial F}{\partial Q}\right\}=\left(\left[\frac{\partial R_s}{\partial Q}\right]^T+\frac{1.5I}{J\Delta t}\right)\Lambda+\left\{\frac{\partial F}{\partial Q}\right\}=\{0\} \tag{9}$$

In order to obtain the solution vector Λ in Eq. (9), the backward Euler implicit method with pseudo time marching is used as:

$$\left(\frac{I}{J\Delta\tau}+\left[\frac{\partial R_s}{\partial Q}\right]^T+\frac{1.5I}{J\Delta t}\right)\Delta\Lambda^{m+1} = -\left(\left[\frac{\partial R_s}{\partial Q}\right]^T+\frac{1.5I}{J\Delta t}\right)\Lambda^m-\left\{\frac{\partial F}{\partial Q}\right\} \tag{10}$$

$$\Lambda^{m+1}=\Lambda^m+\Delta\Lambda^{m+1}$$

The transposed flux Jacobian $[\partial R_s/\partial Q]^T$ in the right-hand size of Eq. (10) is a very large banded matrix requiring a large computer memory. In order to reduce the memory, each element of the adjoint vector Λ is multiplied to the corresponding element of $[\partial R_s/\partial Q]^T$ in the present work. This requires the re-calculation of $[\partial R_s/\partial Q]^T$ at every iteration, and the extra computation time is involved. Nevertheless, this technique is referable to avoid prohibitive memory requirements for large two-dimensional problems and all three-dimensional problems.[4, 7, 12] For efficient calculation of $[\partial R_s/\partial Q]^T$, the residual vector $[\partial R_s/\partial Q]^T$ is differentiated by the primitive variable vector $Q_p=(\rho,u,v,w,p,k,\omega)^T$ rather than by the conservative variable vector Q. Introducing the transformation matrix $M=\partial Q/\partial Q_p$, the transposed flux Jacobian can be calculated by

$$\left[\frac{\partial R_s}{\partial Q}\right]^T=\left(\left[\frac{\partial R_s}{\partial Q_p}\right]\left[\frac{\partial Q_p}{\partial Q}\right]\right)^T=\left[\frac{\partial Q_p}{\partial Q}\right]^T\left[\frac{\partial R_s}{\partial Q_p}\right]^T = M^{-1^T}\left[\frac{\partial R_s}{\partial Q_p}\right]^T \tag{11}$$

The inverse transformation matrix in transposed form is given as:

$$M^{-1^T}=\begin{bmatrix} 1 & -u/\rho & -v/\rho & \frac{(\gamma-1)(u^2+v^2)}{2} & -k/\rho & -\omega/\rho \\ 0 & 1/\rho & 0 & -(\gamma-1)u & 0 & 0 \\ 0 & 0 & 1/\rho & -(\gamma-1)v & 0 & 0 \\ 0 & 0 & 0 & (\gamma-1) & 0 & 0 \\ 0 & 0 & 0 & 0 & 1/\rho & 0 \\ 0 & 0 & 0 & 0 & 0 & 1/\rho \end{bmatrix} \tag{12}$$

For steady-state computations, unsteady time terms in above equations can be vanished by setting the physical time step Δt to be infinity. Details about boundary conditions in the adjoint variable methods are given in Ref. 2.

In the present step, the most difficulty is differentiation of a one- or two-equation turbulence model because of their complicated terms such as the turbulence production and dissipation terms. To reduce the effort to differentiate the turbulence transport equations, the turbulent eddy viscosity μ_T was usually assumed to be constant in the adjoint variable methods.[9, 10] That is, the derivatives of μ_T with respect to the conservative variables Q are set

to zero. Since $d\mu_T / dQ$ is a very large banded matrix of 6 conservative variables at 8 node cells, it requires quite an amount of computer memory. The CTEV assumption saves the computing time as well as computer memory by avoiding the need to solve the differentiated turbulence equations. This assumption, however, may not guarantee the accuracy of the derivatives because it neglects the contribution of the turbulence model to the flow analysis[2, 4].

Results and Discussion

Flow Analysis

Both single- and multi-element airfoils are tested for the validation of the parallel-implemented CFANS2D flow solver[1]. For single airfoil, the transonic flow over the RAE 2822 airfoil is computed at a Mach number of 0.73, a Reynolds number of 6.5×10^6 and an angle of attack 2.79 deg. A 129×65 hyperbolic grid is used with the wall spacing of 1×10^{-5} chord. The computed surface pressure coefficients from the flow solver using the $k-\omega$ SST model[13, 14] are compared with those from the $k-\omega$ model[15, 16], the standard $k-\varepsilon$ model[14], and the experimental data[21] in Fig. 1.

In case of multi-element airfoil, the flow over the NLR7301 airfoil with a 32%c flap is tested at a Mach number of 0.185, a Reynolds number of 2.51×10^6, and an angle of attack of 13.1 deg. The flap is positioned with a deflection angle of 20 deg, an overhang of 5.3%c, and a gap of 2.6%c. A 249×81 hyperbolic grid for the basic airfoil and a 125×41 grid for the flap are used with the wall spacing on the order of 10^{-6} chord in an overlaid grid system. For accurate prediction for higher angles of attack over 13.1 deg, computations are performed in a time-accurate, unsteady manner using the dual time stepping method as already verified in the previous study.[1] The computed surface pressure coefficients using two-equation turbulence models are compared with the experimental data[22] in Fig. 2. Three computed results from different turbulence models show quite a good agreement with experimental one. Figure 3 shows lift coefficients at the wide range of angles of attack from zero to maximum lift. Overall the computed result using the $k-\omega$ SST model yields slightly higher predictions of lift coefficient. However, it shows the capability of the present flow solver to predict the stall angle of 14.1 deg precisely, which is essential in finding $Cl_{\max}$ during the actual high-lift design optimization.

Effects on Sensitivity Analysis

To examine the CTEV assumption more closely, the sensitivity derivatives from the CSAAV code[2] with and without the differentiation of the eddy viscosity are compared in three different flow fields: subsonic and transonic turbulent flows over the RAE 2822 airfoil, and a low-speed turbulent flow over the NLR 7301 with flap at a high angle of attack close to stall angle. In addition, sensitivity gradients of an objective function with respect to design variable using the $k-\omega$ SST model[13, 14] are compared with those using the $k-\omega$ model[15, 16] and the standard $k-\varepsilon$ model[14] to study the effects of turbulence model under the CTEV assumption.

Transonic Airfoil with Strong Shock

To examine the effects of shock discontinuity on sensitivity gradients, the RAE 2822 transonic airfoil is tested at a Reynolds number of 6.5×10^6, an angle of attack of 2.79 deg, and a freestream Mach number of 0.73 where a strong shock wave appears on the upper airfoil surface. The objective to be maximized is set to *lift coefficient*. Angle of attack, α is given as a flow design variable and twenty geometric design variables are also given on both the upper and lower airfoil surfaces using each ten Hicks-Henne functions[23]. In case of a freestream Mach number of 0.73, a strong shock develops on the upper surface of the RAE 2822 airfoil. Figure 4 shows clearly that the CTEV assumption may lead to serious deviations for sensitivity gradients of *lift coefficient* in the turbulent flow involving a strong shock. For the design variable of angle of attack, the deviation reaches up to about 50 percent, and the maximum deviation is as much as 250 percent for the geometric design variables. Since the gradient of flow quantities on the upper airfoil surface is much larger than those on the lower surface, the CTEV assumption causes significant errors mostly on the upper surface. It is also noticed that the level of convergence in both the AV codes with and without the CTEV assumption is at most 3 orders of magnitude of the initial residual.

Effects of Turbulence Models

Three different two-equation turbulence models are tested to examine the effects of turbulence models on sensitivity gradients. Much like the $k-\omega$ SST model, the standard $k-\varepsilon$ and the $k-\omega$ model also show a similar behavior in predicting the sensitivity gradients using both the AV codes as shown in Figs. 5 and 6. The CTEV assumption could yield a significant error since it neglects the very large value of the turbulent eddy viscosity derivative, especially in the downstream adverse pressure gradient region after the shock wave, which directly influences the variation of aerodynamic load coefficients. Therefore it was noted that the contribution of turbulence must be taken into account for the accurate calculations of the sensitivity derivatives in turbulent flows involving strong shocks.[2]

Subsonic Turbulent Airfoil

In this case, the RAE 2822 airfoil is tested again at a freestream Mach number of 0.63, a Reynolds number of 6.5×10^6, and an angle of attack of 2.79 deg. The objective to be maximized is set to lift to drag ratio, C_l / C_d. The sensitivity gradients from the CTEV assumption show some differences with those from the perfect AV code ($\partial\mu_T / \partial Q$ included) as shown in Fig. 7. For the geometric design variables, the maximum deviation of 51 percent occurs near suction peak on the upper surface, whereas the deviation is less than 2 percent for the design variable of angle of attack.

Multielement Airfoil Close to Stall

To demonstrate the capability of the AV code to treat complex geometry, the flow over the NLR7301 airfoil with a 32%c flap is tested at a Mach number of 0.185, a Reynolds number of 2.51×10^6, and an angle of attack of 13.1 deg which is very close to the stall angle of 14.1 deg. As earlier mentioned, the flow information is previously obtained from the unsteady computations in a time-accurate manner using the dual time stepping method. The sensitivity gradients of lift coefficient with respect to angle of attack and geometric changes of the main airfoil and flap are compared in Fig. 8. For the flow variable of angle of attack, the deviation is 40 percent and the largest deviations reach up to 43 and 20 percent on the upper surfaces of main airfoil and flap, respectively. Much like the previous cases, the CTEV assumption causes quite an error in the suction side rather than the pressure side of the high-lift airfoil.

Computing Time and Memory Requirements

The convergence property of the complete AV code is slightly better than that of the AV code with the CTEV assumption as shown in Fig. 9. Computing time and memory requirements of the AV code with the CTEV assumption are compared to those of the complete AV code in Table 1.

Table 1. Comparison of computing time and computer memory requirements.

		AV	AV (μ_T'= 0.)
Single	CPU Time	1.0	0.61
	Memory	1.0	0.36
Multi	CPU Time	1.0	0.57
	Memory	1.0	0.35

This assumption saves both the CPU time and computer memory by about 40 and 65 percent, respectively. In an engineering sense, it might be considerably advantageous to implement this assumption into actual design optimization despite the deficiency of accuracy. However, the side effects of this deficiency of accuracy should be carefully examined in actual design optimization.

Effects on Transonic Design

The CFANS2D flow solver[1] and CSAAV2D sensitivity code[2] are used for single airfoil design optimization through the design procedure in Fig. 10. Optimization is performed using the Broydon-Fletcher-Goldfarb-Shanno (BFGS) variable metric method supported by the DOT (Design Optimization Tool) commercial software[24]. Twenty geometric design variables are given on the upper and lower airfoil surfaces.

To examine the effects of the CTEV assumption on shock discontinuity, the RAE 2822 transonic airfoil is adopted as a baseline model and tested at two different Mach numbers of 0.73 and 0.63, respectively with and without a strong shock wave.

Drag Minimization with Lift Constraint

The RAE 2822 transonic airfoil is adopted as a baseline model and redesigned at a Mach numbers of 0.73, a Reynolds number of 6.5×10^6 and a fixed angle of attack of 2.79 deg. The objective of the first example is to minimize the drag coefficient with a lift constraint. Thus the objective function to be minimized is given by:

$$F = \omega \times Cd + \max(Cl - Cl_0, 0.0) \qquad (13)$$

where Cl_0 is the initial lift coefficient and ω is a weighting value. The initial and designed surface pressure coefficients are compared in Fig. 11. After 12 design iterations, the drag coefficient is reduced from 0.01873 to 0.01357 while the lift coefficient of 0.7895 does not change in Fig. 12. The design case with the complete AV code calls the flow solver 57 times and the sensitivity analysis code 12 times, whereas the design case with the CTEV assumption calls the flow solver 67 times and the sensitivity analysis code 14 times.

Recalling that the AV code with the CTEV assumption gives quite a difference in the gradients of lift coefficient from the perfect AV code as already seen in Fig. 4, it is very interesting that the designed *drag coefficient* using this assumption yields just 2 percent higher deviation than that of the complete design case. This can be explained by that shock wave indicating a non-linear property in transonic flows has disappeared since the second design process, and that the AV code with the CTEV assumption yields a relatively smaller error in the gradients of *drag coefficient* from the perfect AV code in Fig. 13.

Lift Maximization

To examine the effects of the CTEV assumption on shock discontinuity more closely, the second objective is intentionally given to maximize the lift coefficient at a fixed angle of attack, which still admits of a shock wave on the upper surface during all design iterations. Thus the objective function to be maximized is given by:

$$F = Cl \tag{14}$$

Figure 14 shows a dramatic discrepancy in the surface pressure coefficients between two design cases, with and without the CTEV assumption. As already discussed from Fig. 4, it indicates that the incorrect search direction by using this assumption can cause a significant error in the gradient-based design optimization. In the perfect design case, the lift coefficient is increased from 0.7905 to 0.9505 keeping the drag coefficient below 0.02, whereas the lift coefficient is increased from 0.7905 to 0.9445 resulting the drag coefficient over 0.02 in the CTEV design case. Unlike the first example, the designed lift and drag coefficients using the CTEV assumption shows about 1% and 30% error, respectively. Even though not shown here because of space limitations, the $k-\omega$ model and the standard $k-\varepsilon$ model also show similar design results to the $k-\omega$ SST model.

Shock Discontinuity Clearance

To examine the effects of the CTEV assumption on subsonic design involving no shock wave, the RAE 2822 airfoil is adopted again as a baseline model at a Mach number of 0.63, a Reynolds number of 6.5×10^6 and a fixed angle of attack of 2.79 deg. The objective is to maximize the lift to drag ratio and the objective function is simply given by:

$$F = Cl / Cd \tag{15}$$

The designed surface pressure coefficients are shown in Fig. 15. The lift to drag ratio is improved from 57.22 to 64.73 after 3 design iterations, calling the flow solver 21 times and the sensitivity analysis code 3 times. Even though the CTEV assumption also improves the lift to drag ratio to 64.59, its designed surface pressure coefficient and surface geometry are quite different from those of the perfect design case, as already expected from the sensitivity gradients of lift to drag ratio in Fig. 7. Because of the incorrect gradients from the CTEV assumption, a significant error appears mostly on the upper surface. The design example with this assumption calls flow solver 15 times and sensitivity analysis code 2 times, respectively.

Effects on High-Lift Design

The essence of high-lift airfoil design optimization is undoubtedly the improvement of Cl_{max} by modifying the geometric change on each element and varying angle of attack as well. Thus the NLR 7301 airfoil with flap is tested as a baseline model at a Mach number of 0.185, a Reynolds number of 2.51×10^6 and an angle of attack of 13.1 deg. Among total 44 design variables, a flow design variable of angle of attack and 43 geometric variables are given, each 20 on both the upper and lower surfaces of basic airfoil and flap and 3 more geometric changes of flap deflection angle, overlap, and gap. For the accurate prediction of the flow field very close to stall during the one-dimensional search, flow computations are performed in a time-accurate, unsteady manner using the dual time stepping method. The effects of the CTEV assumption on the multielement airfoil design optimization are examined in both cases of landing and take-off configurations at higher angles of attacks close to stall angle.

Take-Off Configuration

The objective of the first example is to maximize the lift to drag ratio at a fixed angle of attack of 13.1 deg. Thus the objective function to be maximized is lift to drag ratio itself as given in Eq. (15). The initial and design surface pressure coefficient distributions are shown in Fig. 16. After 3 design iterations, the lift to drag ratio from the perfect design case is increased from 42.35 to 48.39. Since the initial geometry is originally optimized for take-off configuration, it admits of a little further improvement. The perfect high-lift design case calls flow solver 29 times and sensitivity analysis code 3 times, which indicates that it requires much more flow analyses in one-dimensional search than the transonic design case. The designed lift to drag ratio using the CTEV assumption shows a negligible error of 0.3%.

Maximum-Lift Landing Configuration

The objective of the second example is to maximize the lift coefficient at floating angle of attack. Thus angle of attack is also included as a design variable. The objective function to be maximized is given by Eq. (14). The initial and designed surface pressure coefficients are compared in Fig. 17. For the perfect design using the complete AV code, the angle of attack is extended from 13.1 to 14.17 deg, while it is optimized at 14.03 deg in the CTEV case. The lift coefficients increase from 3.2982 to 3.8862 in the perfect design case and to 3.8399 in the CTEV design case, respectively. However, the perfect design case calls the flow solver 29 times and the sensitivity analysis code 4 times, whereas the CTEV design case calls the flow solver 43 times and the sensitivity analysis code 7 times. It is very interesting that the CTEV design requires more design iterations than the perfect design. This is caused by

the inaccurate information of search direction from the AV code with the CTEV assumption. Figure 18 simulates a substantial improvement of Cl_{max} by vanishing a massively separated flow over a high-lift airfoil using the present design optimization tools.

Total Design Optimization Time

Total design time of the CTEV case is compared to that of the perfect design by the unit of a flow solver running time in Table 2. For the drag minimization of the single airfoil, there are 57 flow solver calls and 12 complete AV code calls, which corresponds to total 114 flow solver calls. Previous bench marks presented that the complete AV code requires 4.8 times more than the flow solver while the AV code with the CTEV assumption requires 2.9 times.[2]

Table 2. Comparison of total design optimization time.

	Design	Flow Solver	AV Code	Total
Single	Perfect	57× 1.0	12× 4.8	114
	CTEV	67× 1.0	14× 2.9	108
Multi	Perfect	29× 1.0	4× 2.0	37
	CTEV	43× 1.0	7× 1.2	51.4

For the Cl_{max} improvement of the multielement airfoil, there are 29 flow solver calls and 4 AV code calls, which corresponds to total 37 flow solver calls. It is noticeable that the CTEV design requires more computing time than the perfect design. Overall the CTEV design requires almost as much computing time as the perfect design in transonic designs, and even more computing time in high-lift designs.

Conclusion

The effects of a usual assumption of constant turbulent eddy viscosity on the aerodynamic design using an adjoint method, one of most efficient gradient-based optimization techniques, are rigorously examined in the present work. Accurate flow analysis is followed by the aerodynamic sensitivity analysis for the Navier-Stokes equations coupled with two-equation turbulence models in a discrete adjoint variable method. The capability of the present sensitivity analysis code to treat complex geometry using the chimera overlaid grid is also demonstrated. Like the mean flow equations, the turbulence model equations are also hand-differentiated to accurately calculate the sensitivity derivatives of flow quantities in turbulent viscous flows. With two-equation turbulence models, it is observed that the constant turbulent eddy viscosity assumption in the adjoint variable method could lead to inaccurate results in several test cases of transonic single airfoil and multielement airfoil. For the accurate computation of the flow over high-lift airfoil close to stall, the unsteady, time-accurate computation is performed using the dual time stepping method. In addition, the effects of constant eddy viscosity assumption on single and multielement airfoil design optimization are carefully investigated in various design examples. It is noted that the perfect AV code gives superior design results to the AV code with the CTEV assumption because of its capability to yield the correct search direction, whereas the CTEV design requires extra design iterations due to its deficiency of accuracy. Consequently it can be deduced that the CTEV assumption might guarantee neither accuracy nor efficiency in the gradient-based optimization, especially for transonic airfoil with strong shock and multielement airfoil at high angle of attack. Above all, the present design tool based on the unsteady CFANS2D solver and the CSAAV2D sensitivity code successfully demonstrates its competency for high-lift design optimization.

Acknowledgment

The present research was supported by the Brain Korea 21 Project.

References

1) Kim, C. S., Kim, C., and Rho, O. H., "Parallel Computations of High-Lift Airfoil Flows Using Two-Equation Turbulence Models," *AIAA Journal*, Vol. 38, No. 8, August 2000, pp. 1360-1368.

2) Kim, C. S., Kim, C., and Rho, O. H., "Sensitivity Analysis for the Navier-Stokes Equations with Two-Equation Turbulence Models," *AIAA Journal*, Vol. 39, No. 5, May 2001, pp. 838-845.

3) Eyi, S., and Lee, K. D., "Effect of Sensitivity Calculation on Navier-Stokes Design Optimization," AIAA 94-0060, Jan. 1994.

4) Nielsen, E. J., and Anderson, W. K., "Aerodynamic Design Optimization on Unstructured Meshes Using the Navier-Stokes Equations," AIAA 98-4809, Jan. 1998.

5) Eleshaky, M. E., and Baysal, O., "Aerodynamic Shape Optimization Using Sensitivity Analysis on Viscous Flow Equations," Journal of Fluid Engineering, Vol. 115, No.3, 1993, pp. 75-84.

6) Ajmani, K., and Taylor, A. C. III, "Discrete Sensitivity Derivatives of the Navier-Stokes Equations with a Parallel Krylov Solver," AIAA 94-0091, Jan. 1994.

7) Sherman, L. L., Taylor, A. C. III, Green, L. L., Newman, P. A., Hou, G. J., and Korivi, V. M., "First- and Second-Order Aerodynamic Sensitivity Derivatives via Automatic Differentiation with Incremental Iterative Methods," AIAA-94-4262-CP, Sep. 1994.

8) Mohammadi, B, "Optimal shape Design, Reverse Mode

of Automatic Differentiation and Turbulence," AIAA 97-0099, Jan. 1997.

9) Jameson, A., Pierce, N. A., and Martinelli, L., "Optimum Aerodynamic Design Using the Navier-Stokes Equations," AIAA 97-0101, Jan. 1997.

10) Soemarwoto, B. I., "The Variational Method for Aerodynamic Optimization Using the Navier-Stokes Equations," NASA/CR-97-206277, ICASE Report No. 97-71, Dec. 1997.

11) Taylor, A. C. III, and Osolo, A., "Aerodynamic Design Sensitivities By Automatic Differentiation," AIAA 98-2536, June 1998.

12) Kim, H. J., Kim, C. A., Rho, O. H., and Lee, K. D., "Aerodynamic Sensitivity Analysis For Navier-Stokes Equations," AIAA 99-0402, Jan. 1999.

13) Menter, F. R., "Influence of Freestream Values on the $k-\omega$ Turbulence Model Predictions," *AIAA Journal*, Vol. 30, No. 6, August 1992, pp. 1651-1659.

14) Menter, F. R., "Two-Equation Eddy-Viscosity turbulence Models for Engineering Applications," *AIAA Journal*, Vol. 32, No. 8, August 1994, pp. 1598-1605.

15) Wilcox, D. C., "Reassessment of the Scale-Determining Equation for Advanced Turbulence Models," *AIAA Journal*, Vol. 26, No. 11, 1988, pp. 1299-1310.

16) Wilcox, D. C., "Simulation of Transition with a Two-Equation Turbulence Model," *AIAA Journal*, Vol. 32, No. 2, Feb. 1994, pp. 247-255.

17) Kim, C. S., "Sensitivity Analysis for the Navier-Stokes Equations with Two-Equation Turbulence Models and Its Applications," Ph.D. Dissertation, Seoul National University, Seoul, Korea, 2001.

18) Roe, P. L., "Approximate Riemann Solvers, Parameter Vectors and Difference Schemes," Journal of Computational Physics, Vol.43, 1981, pp.357-372.

19) Hwang, S. W., "Numerical Analysis of Unsteady Supersonic Flow over Double Cavity," Ph.D. Dissertation, Seoul National University, Seoul, Korea, 1996.

20) Yoon, S., and Kwak, D., "Three-Dimensional Incompressible Navier-Stokes Solver Using Lower-Upper Symmetric-Gauss-Seidel Algorithm," *AIAA Journal*, Vol. 29, June 1991, pp. 874-875.

21) Cook, P. H., McDonald, M. A., and Firmin, M. C. P., "Aerofoil RAE 2822 – Pressure Distributions, and Boundary Layer and Wake Measurements," AGARD AR 138, May 1979, A6-1 to A6-77.

22) Berg, B. v. d., "Boundary Layer Measurements On a Two-Dimensional Wing With Flap," NLR TR 79009 U, Jan. 1979.

23) Hicks, R. M. and Henne, P. A., "Wing Design by Numerical Optimization," *Journal of Aircraft*, Vol.15, No.7, 1978, pp. 407-412.

24) DOT Users Manual, Version 4.00, VMA Engineering, Vanderplaats, Miura & Associate, Inc., 1993.

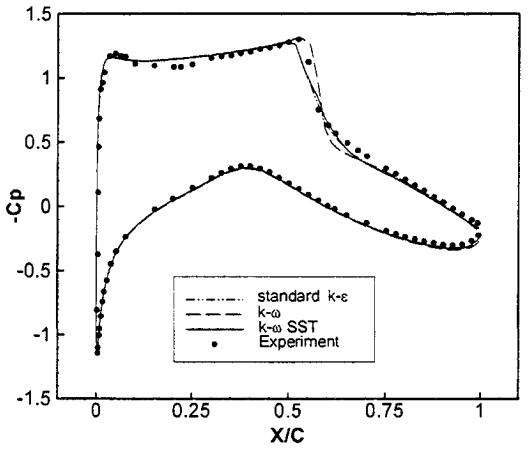

Fig. 1 Surface pressure coefficients over the RAE 2822 airfoil at α=2.79 deg, M=0.73, and Re= 6.5×10^6.

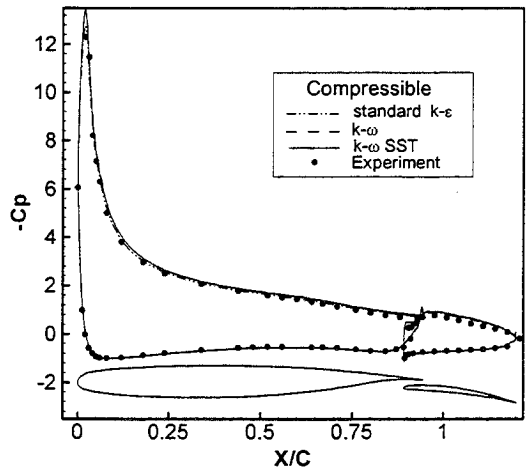

Fig. 2 Surface pressure coefficients over the NLR 7301 airfoil with flap at α=13.1 deg, M=0.185, and Re= 2.51×10^6.

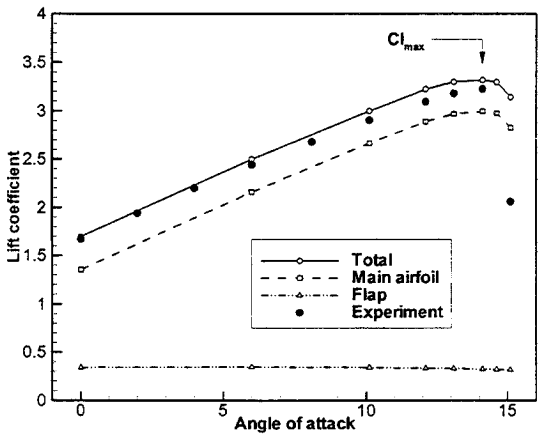

Fig. 3 Lift coefficient vs. angle of attack for the NLR 7301 airfoil with flap.

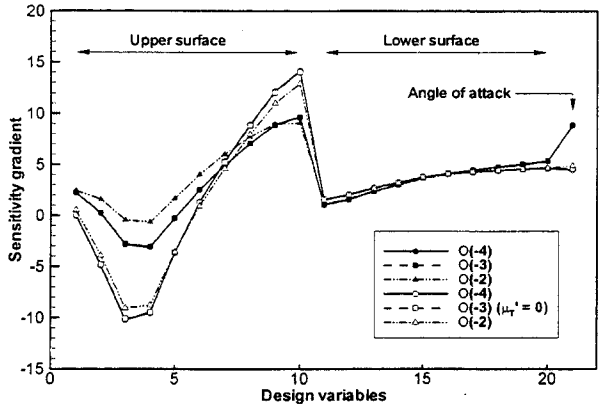

Fig. 4 Convergence of sensitivity gradients of lift coefficient at M=0.73: $k-\omega$ SST model.

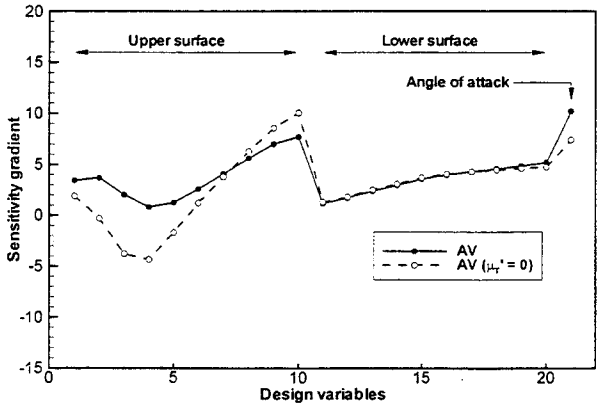

Fig. 5 Sensitivity gradients of lift coefficient at M=0.73: $k-\varepsilon$ model.

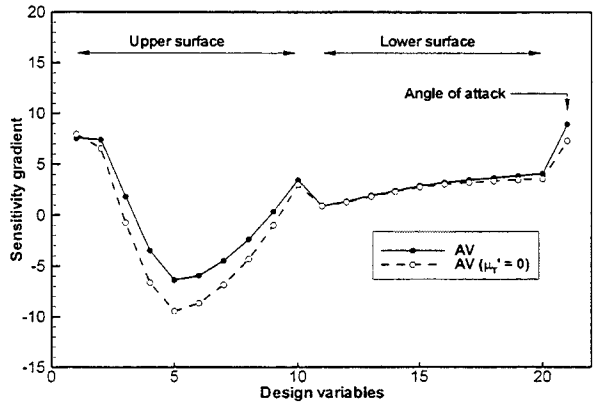

Fig. 6 Sensitivity gradients of lift coefficient at M=0.73: $k-\omega$ model.

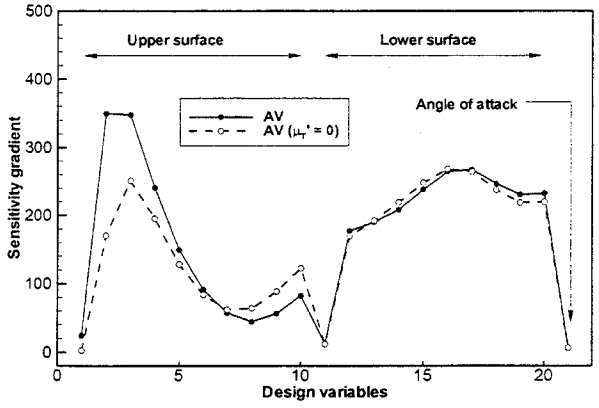

Fig. 7 Sensitivity gradients of lift to drag ratio at M=0.63: $k-\omega$ SST model.

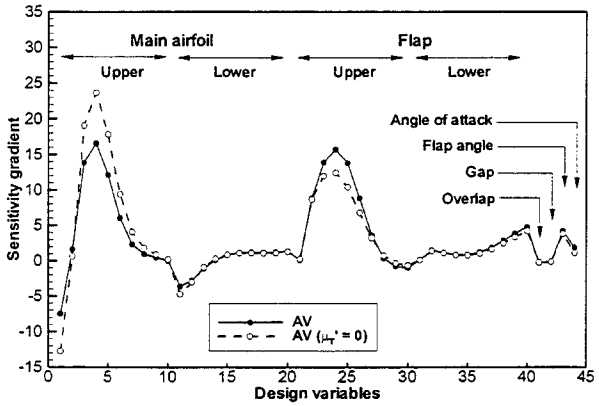

Fig. 8 Sensitivity gradients of lift coefficient at M=0.185: NLR 7301 airfoil with flap.

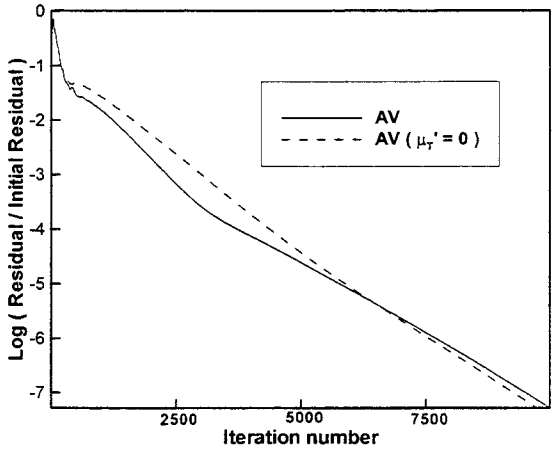

Fig. 9 Comparison of convergence histories.

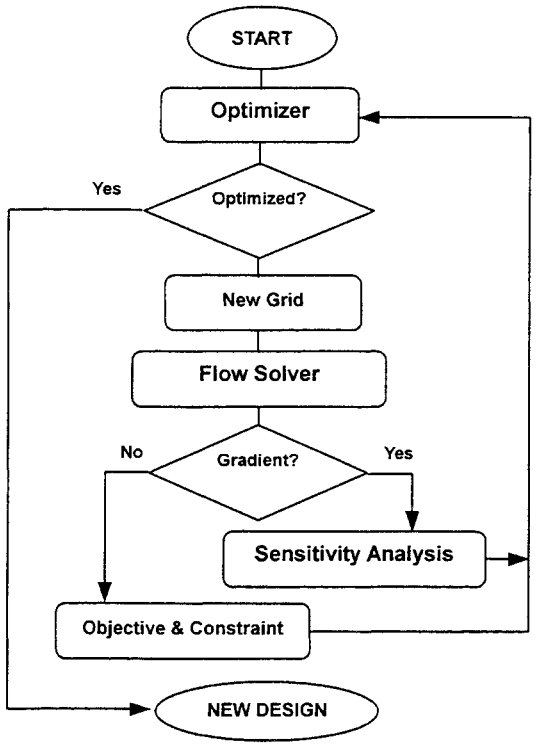

Fig. 10 Flow chart of a gradient-based design optimization.

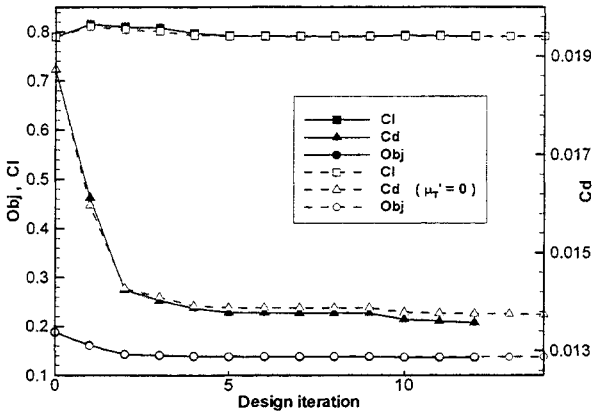

Fig. 12 Design progress of drag minimization with lift constraint at M=0.73.

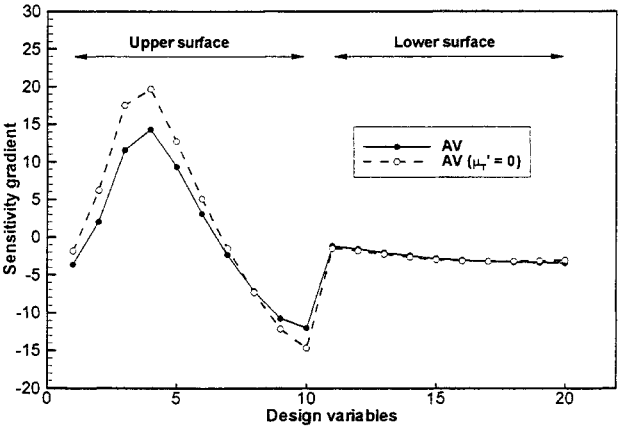

Fig. 13 Sensitivity gradients for drag minimization with lift constraint.

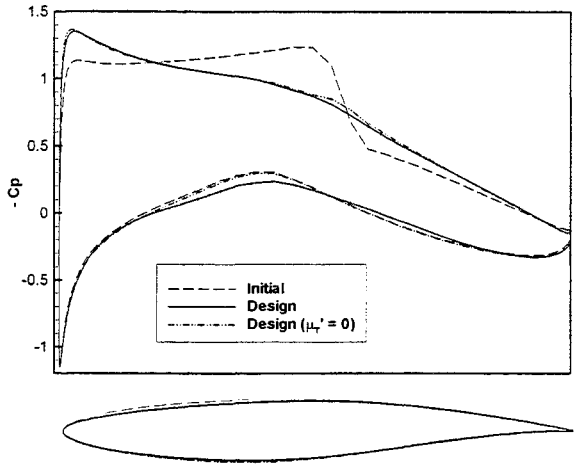

Fig. 11 Drag minimization with lift constraint for single airfoil at M=0.73.

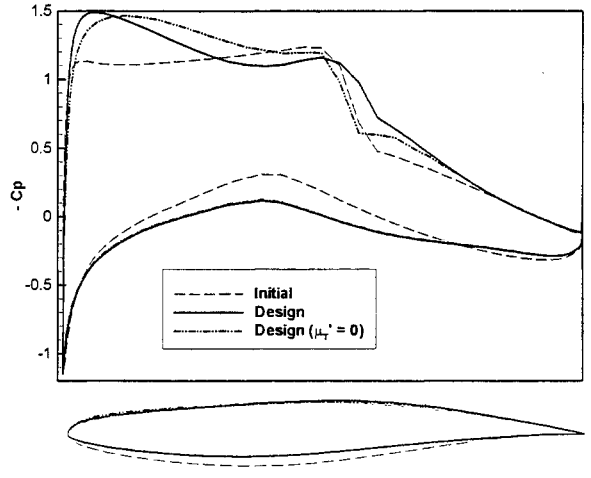

Fig. 14 Lift maximization using the $k-\omega$ SST turbulence model.

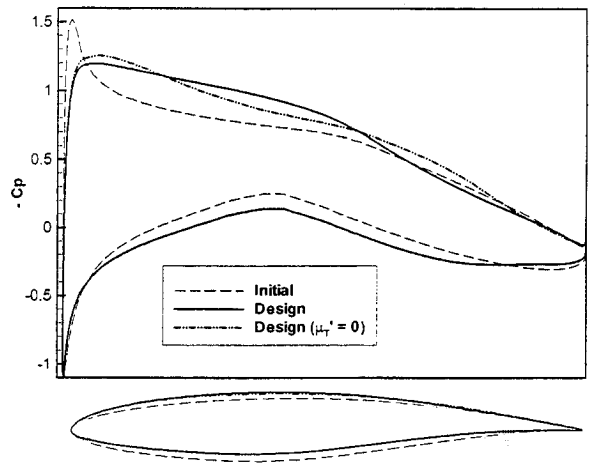

Fig. 15 Lift to drag maximization for single airfoil at M=0.63.

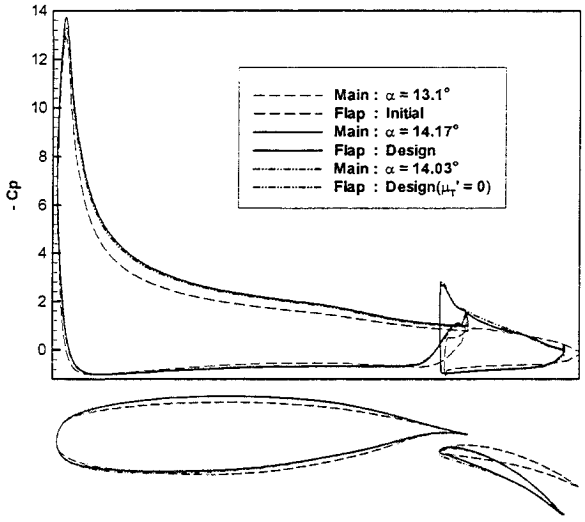

Fig. 17 Improvement of $Cl_{\max}$ for multielement airfoil.

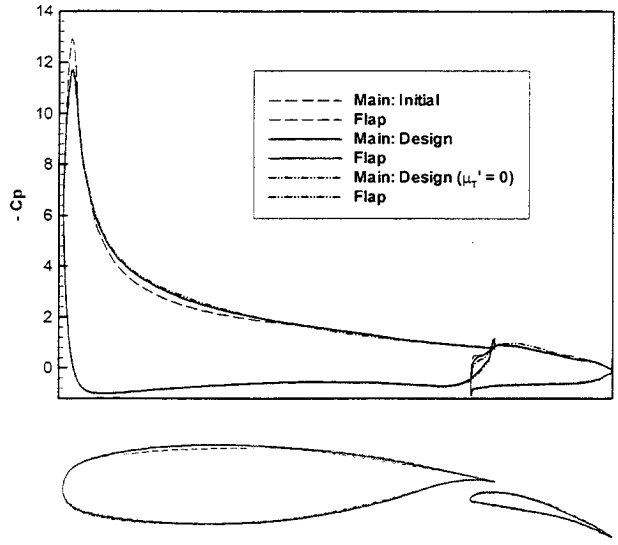

Fig. 16 Lift to drag maximization for multielement airfoil.

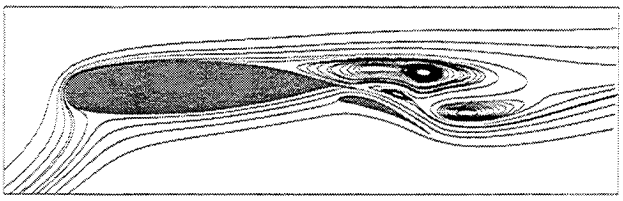

(a) Massively separated flow during design

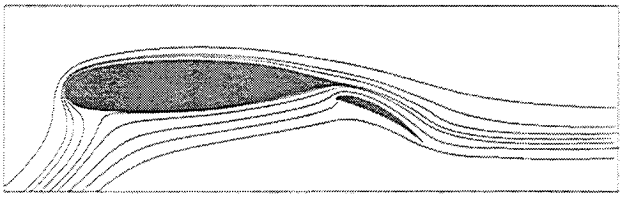

(b) Attached flow after design

Fig. 18 Comparison of streamlines over high-lift airfoil with flap.